


Rainbow scars: From area to volume lawChristopher M. Langlett,¹ Zhi-Cheng Yang^{2,3}, Julia Wildeboer,⁴ Alexey V. Gorshkov^{2,3},
Thomas Iadecola^{4,*} and Shenglong Xu^{1,†}¹*Department of Physics & Astronomy, Texas A&M University, College Station, Texas 77843, USA*²*Joint Center for Quantum Information and Computer Science, NIST/University of Maryland, College Park, Maryland 20742, USA*³*Joint Quantum Institute, NIST/University of Maryland, College Park, Maryland 20742, USA*⁴*Department of Physics & Astronomy, Iowa State University, Ames, Iowa 50011, USA* (Received 26 July 2021; revised 10 November 2021; accepted 21 January 2022; published 7 February 2022)

Quantum many-body scars (QMBS) constitute a new quantum dynamical regime in which rare “scarred” eigenstates mediate weak ergodicity breaking. One open question is to understand the most general setting in which these states arise. In this work, we develop a generic construction that embeds a new class of QMBS, rainbow scars, into the spectrum of an *arbitrary* Hamiltonian. Unlike other examples of QMBS, rainbow scars display extensive bipartite entanglement entropy while retaining a simple entanglement structure. Specifically, the entanglement scaling is volume-law for a random bipartition, while scaling for a fine-tuned bipartition is subextensive. When internal symmetries are present, the construction leads to multiple, and even towers, of rainbow scars revealed through distinctive non-thermal dynamics. Remarkably, certain symmetries can lead rainbow scars to arise in translation-invariant models. To this end, we provide an experimental road map for realizing rainbow scar states in a Rydberg-atom quantum simulator, leading to coherent oscillations distinct from the strictly sub-volume-law QMBS previously realized in the same system.

DOI: [10.1103/PhysRevB.105.L060301](https://doi.org/10.1103/PhysRevB.105.L060301)

Introduction. Statistical mechanics relies on relaxation towards the maximally entropic state in thermal equilibrium. This process, however, is at odds with the fact that the entropy of a many-body system prepared in a pure state must remain identically zero under unitary dynamics. The emergence of statistical mechanics in such systems, known as quantum thermalization, proceeds by the relaxation of local subregions to a thermal state via the exchange of quantum correlations with the remainder of the system. This mechanism, whereby a pure state becomes locally indistinguishable from a thermal state, follows from the eigenstate thermalization hypothesis (ETH) [1–4]. The ETH postulates a correspondence between the local reduced density matrix of a finite-energy-density eigenstate and the Gibbs ensemble.

Many lines of inquiry involve constructing systems where thermalization is avoided. For example, quantum integrable systems [5,6] fail to thermalize due to extensively many conservation laws; however, these systems are unstable to perturbations. A more robust violation of the ETH arises in disordered interacting systems, which may induce many-body localization, resulting in an extensive number of conservation laws [7–10].

Experiments utilizing cold atoms [11–16], ion traps [17,18], and superconducting circuits [19,20] demonstrated unprecedented control over the dynamics of many-body systems. Recently, experiments in Rydberg-atom arrays simulating quantum Ising models in varying dimensions [21,22]

observed sustained coherent oscillations of local observables for special initial states, such as the Néel state. This observation was later traced to the existence of rare, weakly entangled eigenstates in an otherwise thermal system [23,24]. This phenomenology was dubbed “quantum many-body scars” (QMBS) [25], an earlier example of which was found in the Affleck-Kennedy-Lieb-Tasaki spin chain in Refs. [26,27]. QMBS have been studied in a wide range of systems, including the “*PXP* model” simulated by the Rydberg experiment [28–32], the spin-1 *XY* model [33,34], Fermi-Hubbard models [35,36], Floquet models [37–41], and other systems [42–52]. Group-theoretic techniques [35,53–57], matrix product state methods [58], and projector embeddings [59,60] have been employed to systematically generate sub-volume-law QMBS in the many-body spectrum. It remains an open question to construct QMBS with a specific entanglement structure in the spectrum of a generic system.

In this work, we develop a general construction for a new class of QMBS, rainbow scars [61–63], in the spectrum of an *arbitrary* Hamiltonian governing a replicated system. Rainbow scars differ from previous examples of QMBS in that their entanglement scaling strongly depends on the chosen bipartition. Specifically, the entanglement is volume-law for a random cut, but sub-volume-law for a fine-tuned cut. In the presence of symmetries, multiple and even towers of rainbow scar states emerge, and may exhibit a rich group-theoretic structure. This opens the possibility to probe the scar states with quantum quenches. Furthermore, certain symmetries can even yield rainbow scars in simple translation-invariant models. We propose a realization of rainbow scars in a system of interacting Rydberg atoms, where these states lead to coherent

*iadecola@iastate.edu

†slxu@tamu.edu

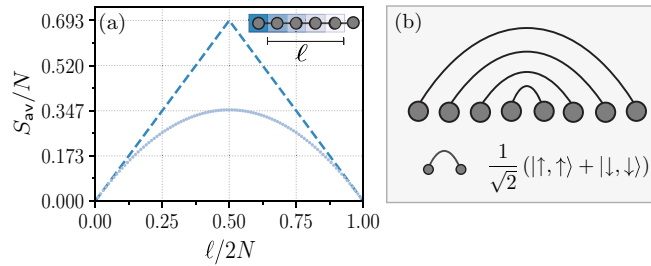


FIG. 1. Entanglement scaling of the random bipartition is shown. (a) Average entanglement for each bipartition $\ell \in [0, 2N]$, the dotted line indicates maximal entanglement, here $2N = 200$. Inset: Depiction of bipartitions. (b) Rainbow state for $d = 2$ with each bond a Bell state.

oscillatory dynamics whose origin is fundamentally distinct from the previously studied sub-volume-law QMBS.

General construction. Imagine two related copies of a quantum many-body system with the Hamiltonian

$$H = H_1 \otimes \mathbb{1} + \mathbb{1} \otimes H_2 + \lambda_c V_c. \quad (1)$$

Each subsystem H_1 and H_2 consists of N sites with a d -dimensional local Hilbert space, spanned by the local computational basis $|s_i\rangle$ at site i . The state $|S\rangle = \prod_i |s_i\rangle$ defines the global computational basis spanning a Hilbert space of dimension d^{2N} . Moreover, in one dimension [64], the “copied” Hamiltonian, H_2 , satisfies $H_2 = -MH_1^*M$, with the mirror-symmetry operator M mapping $i \rightarrow \tilde{i} \equiv 2N - i + 1$. Complex conjugation is defined with respect to the computational basis $|S\rangle$. The two systems interact through V_c , which generically thermalizes the combined system, akin to two boxes of gas equilibrating through a thin connecting wire. Provided the condition $H_2 = -MH_1^*M$ is met, the construction is independent of the microscopic details of $H_{1(2)}$. This strict condition on H_2 is relaxed in the presence of certain symmetries, as discussed below.

We proceed by illustrating how a class of nonthermal states emerges from a large set of degenerate states through a carefully chosen coupling. Using the spectral decomposition to express $H_1 = \sum_{n=1}^{d^N} E_n |\psi_n\rangle \langle \psi_n|$, where $H_1 |\psi_n\rangle = E_n |\psi_n\rangle$, and similarly express $H_2 = -\sum_{n=1}^{d^N} E_n |\mathcal{M}\psi_n^*\rangle \langle \mathcal{M}\psi_n^*|$, where $|\mathcal{M}\psi_n^*\rangle \equiv (\mathcal{M}|\psi_n\rangle)^*$. At $\lambda_c = 0$, the eigenstates of the total Hamiltonian H , with eigenvalues $E_n - E_m$, are $\{|\Psi_{nm}\rangle = |\psi_n\rangle \otimes |\mathcal{M}\psi_m^*\rangle : \forall n, m = 1, \dots, d^N\}$, which have no entanglement between the two halves. Consequently, H has a d^{2N} -fold degenerate subspace spanned by $|\Psi_{nm}\rangle$. Within this degenerate subspace, there exists a special eigenstate independent of the details of H_1 :

$$|I\rangle = \frac{1}{d^{N/2}} \sum_{n=1}^{d^N} |\Psi_{nn}\rangle = \frac{1}{d^{N/2}} \bigotimes_{i=1}^N \sum_{s=0}^{d-1} |s_i\rangle |s_{\tilde{i}}\rangle, \quad (2)$$

where the second equality follows from inserting a resolution of the identity. This state is precisely the “rainbow state” [61–63], named for its characteristic pattern of entanglement, in which every site i is maximally entangled with its mirror partner \tilde{i} [see Fig. 1(b), middle inset]. The rainbow state is also known as the infinite-temperature thermofield double

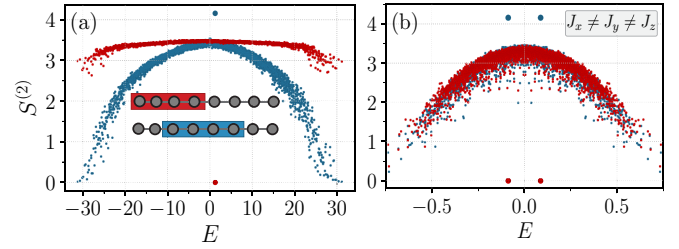


FIG. 2. Second-order Rényi entropy is depicted. (a) Second-order Rényi entropy for a random Hamiltonian drawn from the GUE with a Heisenberg coupling $\lambda_c = 5.0$. (Inset) Chosen entanglement cuts: standard bipartition (blue) and fine-tuned bipartition (red). (b) Translation-invariant model with $J_x = 0.20$, $J_y = 0.15$, $J_z = 0.25$ using open boundary conditions.

state; it is of interest in the high-energy community [65–68] for its connections to black-hole physics and in the quantum information community where it is used as an entanglement resource [69–71]. The entanglement entropy for the standard bipartition [see Fig. 2(a), top inset] scales linearly with system size $S = N \log d$, while retaining a simple structure. More generally, for a random bipartition defining a subregion A of size ℓ , the entanglement scales extensively on average when $\ell \propto N$: $S_{\text{av}} = (2N - \ell)\ell \log(d)/(2N - 1)$ [Fig. 1(a)] [see Supplementary Material (SM) [72]]. The rainbow state is denoted as the state $|I\rangle$ corresponding to the identity operator under the state-channel duality [73,74]. For $\lambda_c \neq 0$, the rainbow state is selected as an eigenstate of the local Hamiltonian H from the degenerate subspace provided $|I\rangle$ is an eigenstate of V_c . Specifically, for $d = 2$, $|I\rangle$ is a product of long-range Bell states, $|I\rangle = \bigotimes_{i \leq N} (|\uparrow, \uparrow\rangle + |\downarrow, \downarrow\rangle)_{i, \tilde{i}}$. If the subsystems are coupled through, e.g., a Heisenberg interaction, $V_c = \vec{S}_N \cdot \vec{S}_{N+1}$, then $|I\rangle$ is an eigenstate of the combined system with energy $E_I = \lambda_c/4$.

To emphasize the generality of the construction, consider a system of $2N$ qubits for which H_1 (which fixes H_2) is randomly drawn from the Gaussian unitary ensemble (GUE), with a local Heisenberg coupling acting on the central qubits. Figure 2(a) shows the second-order Rényi entropy $S^{(2)} \equiv -\log \text{tr}(\rho_A^2)$, for each eigenstate of H , where ρ_A is the reduced density matrix of subregion A for two different entanglement cuts. Blue points denote the standard bipartition, while the red points denote the fine-tuned bipartition [see Fig. 2(a), inset]. The appearance of a “thermalization band” [75–79] in both cases indicates that the coupling brings the combined system to equilibrium, as expected for a random chaotic model. Additional evidence is obtained through the average level spacing parameter [9,80–82], $\langle r \rangle \sim 0.594$, which falls near the GUE random matrix result, 0.60 [83]. For the standard bipartition, the rainbow state is found as a nondegenerate eigenstate above the band with maximal entanglement, markedly distinct from previous examples of QMBS. By contrast, for the fine-tuned bipartition, the rainbow state is a product state, thus violating expectations from ETH. *A priori*, a random chaotic model is not expected to host QMBS; nevertheless, the local Heisenberg coupling between the two copies is responsible for selecting $|I\rangle$ from the degenerate subspace and elevating it to a scar.

Symmetries. First, we discuss how an appropriate symmetry relaxes the condition on H_2 . Consider a system with a spectral-reflection symmetry [84] implemented by an operator \mathcal{O} satisfying $\{\mathcal{O}, H_1\} = 0$. We can then define $H_2 = +\mathcal{M}H_1^*\mathcal{M}$ and the state $|\mathcal{O}\rangle = (\mathcal{O} \otimes \mathbb{1})|I\rangle$ as an eigenstate of $H_1 \otimes \mathbb{1} + \mathbb{1} \otimes H_2$. This symmetry can even be used to realize the construction in fully translation-invariant models. For instance, consider the Hamiltonian

$$H = \sum_{i=1}^{2N-1} (J_x S_i^x S_{i+1}^x + J_y S_i^y S_{i+1}^y) + \sum_{i=1}^{2N-2} J_z S_i^z S_{i+1}^z S_{i+2}^z, \quad (3)$$

where S_i^α are the standard spin- $\frac{1}{2}$ operators on site i . The Hamiltonian above reduces to the form of Eq. (1) through a unitary transformation with the operator $\mathcal{O} = \prod_{i=1}^N \sigma_{N+i}^x \sigma_{N+i+1}^y$ which flips the sign of the Hamiltonian on the last N sites. Here the coupling becomes $\lambda_c V_c = J_x S_N^x S_{N+1}^x + J_y S_N^y S_{N+1}^y + J_z (S_{N-1}^z S_N^z S_{N+1}^z - S_N^z S_{N+1}^z S_{N+2}^z)$, for which the rainbow state $|I\rangle$ is an eigenstate. As discussed above, the state $|\mathcal{O}\rangle$ then becomes an eigenstate of Eq. (3). Figure 2(b) shows $S^{(2)}$ for each eigenstate of Eq. (3) revealing two rainbow scars; the mechanism for multiple scars is elaborated below.

Symmetries enrich the construction to yield multiple rainbow scar states, which is why two rainbow scars appear in the previous example. Let \mathcal{O}^α be symmetry generators satisfying $[H_1, \mathcal{O}^\alpha] = 0$. Then the state $|\mathcal{O}^\alpha\rangle = (\mathcal{O}^\alpha \otimes \mathbb{1})|I\rangle$ also belongs to the d^N -fold degenerate subspace at $\lambda_c = 0$ and is independent of the details of H_1 . Provided the $|\mathcal{O}^\alpha\rangle$ are eigenstates of V_c , they will emerge as scars in the spectrum. For example, consider the case where H_1 has a \mathbb{Z}_2 symmetry generated by $\mathcal{O}^x = \prod_{i \leq N} \sigma_i^x$, where σ^x is a Pauli operator. The result is an additional rainbow state, $|X\rangle = \bigotimes_{i \leq N} (|\downarrow, \uparrow\rangle + |\uparrow, \downarrow\rangle)_{i, \bar{i}}$. If $[H_1, \mathcal{O}^\alpha] = 0$ for each $\mathcal{O}^\alpha = \prod_{i \leq N} \sigma_i^\alpha$ ($\alpha = \{x, y, z\}$), then a set of orthogonal rainbow scars, $\{|I\rangle, |X\rangle, |Y\rangle, |Z\rangle\}$ arises in the spectrum. Moreover, an extensive number of rainbow scars emerge if H possesses a global symmetry or kinetic constraints leading to disconnected subsectors.

We examine the consequence of symmetries by studying two coupled XYZ chains of N spins:

$$H_1 = \sum_{i=1}^{N-1} J_x S_i^x S_{i+1}^x + J_y S_i^y S_{i+1}^y + J_z S_i^z S_{i+1}^z + \tilde{J} S_i^z S_{i+2}^z. \quad (4)$$

The next-nearest neighbor interaction \tilde{J} is included to prevent integrability. H_2 is set to $-\mathcal{M}H_1^*\mathcal{M}$, and the chains are coupled by $V_c = \tilde{S}_N \cdot \tilde{S}_{N+1}$.

If H_1 commutes with \mathcal{O}^α for $\alpha = \{x, y, z\}$, then four orthogonal rainbow scar states, $\{|I\rangle, |X\rangle, |Z\rangle, |Y\rangle\}$, emerge as eigenstates of H . The first three states correspond to the triplet states of V_c and are degenerate with energy $\lambda_c/4$, while the final state is the singlet state of V_c at energy $-3\lambda_c/4$.

When $J_x = J_y$, the total magnetization $S^z = \sum_{i=1}^{2N} S_i^z$ of the combined system is conserved. In this case, the four scar states discussed above are still present, and their projections into each magnetization sector (if nonzero) are eigenstates. For instance, the states $|X\rangle$ and $|Y\rangle$ lie within the $S^z = 0$ sector. $|I\rangle$ and $|Z\rangle$, instead, have finite projections onto all magnetization sectors with $\sum_{i=1}^N S_i^z = \sum_{i=N+1}^{2N} S_i^z$; these pro-

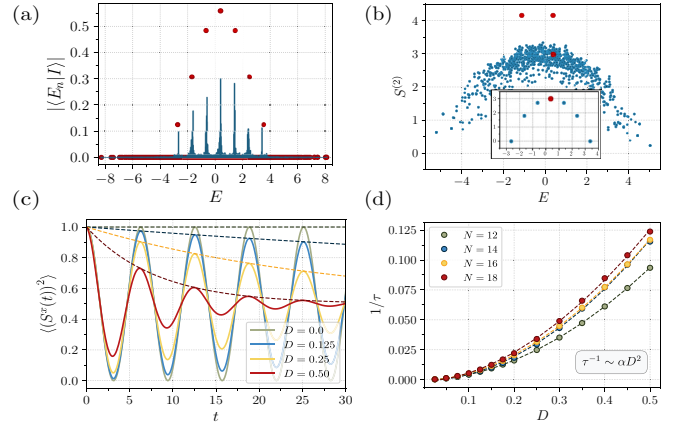


FIG. 3. U(1) tower of rainbow scars. (a) Overlap between the rainbow state $|I\rangle$ and each energy eigenstate of Eq. (4), both with ($J_x = J_y = 1.0$, red) and without ($J_x = 1.0, J_y = 1.25$, blue) U(1) symmetry. (b) Second-order Rényi entropy using the standard bipartition within the $S^z = 0$ sector in the U(1)-symmetric case ($J_x = J_y = 1.5$). Inset: The tower highlights the doubly degenerate projected rainbow states $|I\rangle$ and $|Z\rangle$ in each allowed magnetization sector (red dot indicates $S^z = 0$). (c) Krylov time evolution of $\langle (S^x(t))^2 \rangle / N$ in a system of $2N = 18$ spins prepared in $|I\rangle$, with time step $dt = 0.1$. The dotted lines are fits capturing the amplitude decay. (d) Inverse lifetime of $\langle (S^x(t))^2 \rangle / N$ with increasing perturbation strength. The remaining parameters used in (a)–(d) are $J_z = 2.0, \mu = 0.5, \tilde{J} = 0.5, \lambda_c = 1.5$.

jections coincide up to a global phase, leading to $N + 1$ degenerate eigenstates. Adding μS^z breaks this degeneracy, resulting in an equally spaced tower of scar states. This tower of states is created by applying $\hat{J}^+ = \sum_{i=1}^N S_i^+ S_i^+$ to the fully polarized state $|\Omega\rangle = \bigotimes_i |\downarrow\rangle$. Together with $\hat{J}^z = \frac{1}{2} \sum_{i=1}^{2N} S_i^z$, one can readily verify that the operators \hat{J}^\pm and \hat{J}^z obey $SU(2)$ commutation relations, so that the tower forms a spin- $N/2$ representation of $SU(2)$. In Fig. 1(b), we plot $S^{(2)}$ for each eigenstate with $S^z = 0$, with the nonthermal states spanning the tower in the inset. The states $\{|X\rangle, |Y\rangle\}$ in the $S^z = 0$ sector are nonzero because they are exact eigenstates of the magnetic field term [85]. In Ref. [72], we demonstrate that the tower has volume-law entanglement scaling for the standard bipartition and logarithmic scaling for the fine-tuned cut.

Performing a quantum quench from an initial state with finite weight on each eigenstate of the tower leads to perfect coherent dynamics [53,55–57]. In particular, preparing Eq. (4) in either $|I\rangle$ or $|Z\rangle$ results in perfect oscillations, quantified through the nonlocal correlator, $\langle (S^x(t))^2 \rangle / N$ for $2N = 20$ spins, where $S^x = \sum S_i^x$. These oscillations are found to be remarkably robust to perturbations. We perturb Eq. (4) by setting $J_y - J_x = D$ [86]; at $D = 0$, the U(1) symmetry is exact and the correlator has the analytical form $\langle (S^x(t))^2 \rangle / N = \langle S^x(0)^2 \rangle \cos^2(\mu t) / N$. For $D \neq 0$, the U(1) symmetry is explicitly broken; yet, the oscillations remain strong for deviations up to $D \sim 0.50$, upon which thermalization sets in [see Fig. 3(c)]. We find that the inverse lifetime $1/\tau \sim \alpha D^2$, where $\alpha \approx 0.40$, as expected from Fermi's golden rule [see Fig. 3(d)]. Perturbations like D that preserve the structure of Eq. (1) yield a more robust dynamical signature than

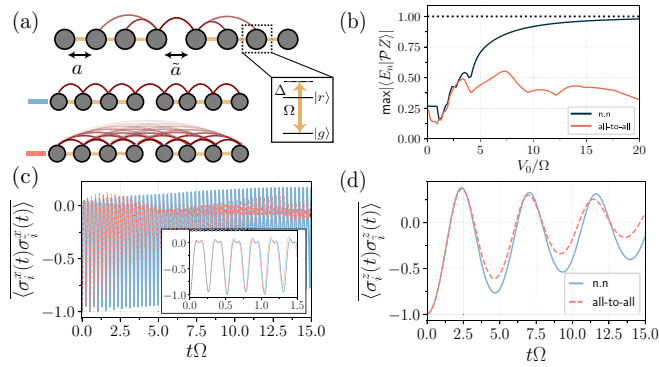


FIG. 4. Dynamical signature in a chain of interacting Rydberg atoms. (a) Depiction of a nonuniformly spaced Rydberg chain. (b) Maximum overlap of $|Z\rangle$ projected into the subsector absent of neighboring Rydberg states for different interaction strengths. Nearest-neighbor (all-to-all) interactions are denoted by blue (red). (c) Dynamics of the average expectation value between inversion pairs $\langle \sigma_i^x(t) \sigma_i^x(t) \rangle$ prepared in $|Z\rangle$. Inset: Short time dynamics for $t\Omega \sim 1.5$. (d) Néel state dynamics for the correlator, $\langle \sigma_i^z(t) \sigma_i^z(t) \rangle$. Parameters used in (b)–(d): $\Omega/2\pi = 2\text{MHz}$, $V_0 = 12\Omega$, $\Delta_{\text{opt}} = V_0/2\tilde{a}^6$ with $\tilde{a} \sim 1.51$ and $2N = 16$.

perturbations that break not only $U(1)$ but also the form of Eq. (1) [72].

Experimental realization. As a physically motivating example, we consider a chain of interacting Rydberg atoms with a nonuniform spacing [see Fig. 4(a)] governed by the Hamiltonian

$$H = \frac{\Omega}{2} \sum_{i=1}^{2N} \sigma_i^x + \sum_{i < j} V_{i,j} n_i n_j - \sum_{i=1}^{2N} \Delta_i n_i. \quad (5)$$

Here we set the interatomic spacing $a = 1$ except between sites N and $N + 1$, where the spacing is \tilde{a} . The operator σ_i^x connects the internal ground state $|g\rangle_i$ to the Rydberg state $|r\rangle_i$ of the i th atom, with parameters Ω (Rabi frequency) and Δ_i (detuning) characterizing the drive laser. Rydberg states interact through $V_{i,j} = V_0/r_{i,j}^6$, with operators $n_i = (1 + \sigma_i^z)/2$. In the limit $V_{i,i+1} \gg \Omega \gg V_{i,i+2}$, we take $V_{N,N+1} = V_0/\tilde{a}^6$ to be comparable to Ω ; equivalently, we take $\tilde{a} > 1.0$. In addition, we take $\Delta_i = 0$ except for the two central sites, where $\Delta_N = \Delta_{N+1} = \Delta_{\text{opt}} = V_{N,N+1}/2$. The coupling then becomes $V_0 \sigma_N^z \sigma_{N+1}^z / 4\tilde{a}^6$.

In the limit $V_{i,i+1} \gg \Omega \gg V_{i,i+2}$, a pair of $U(1)$ conservation laws emerge, with generators $n_{1(2)}^{rr} = \sum_{i(\tilde{i})=1}^N n_{i(\tilde{i})} n_{i(\tilde{i})+1}$ that count the number of nearest-neighbor pairs of Rydberg excitations in each half of the chain. The projection of H onto a sector with fixed $n_{1,2}^{rr}$ reads

$$H = H_1 + H_2 + \frac{V_0}{4\tilde{a}^6} \sigma_N^z \sigma_{N+1}^z + V_0 (n_1^{rr} + n_2^{rr}), \quad (6)$$

with $H_{1(2)} = \mathcal{P}_{1(2)} (\frac{\Omega}{2} \sum_{i=1}^N \sigma_i^x) \mathcal{P}_{1(2)}$ where $\mathcal{P}_{1(2)}$ projects the left (right) half of the chain into a sector with fixed $n_{1(2)}^{rr}$. The Hamiltonians $H_{1(2)}$ individually have a spectral-reflection symmetry since $\{\mathcal{O}^z, H_{1(2)}\} = 0$ [87] When $\mathcal{P}_1 = \mathcal{M}\mathcal{P}_2\mathcal{M}$ (note $\mathcal{P}_1^* = \mathcal{P}_1$), then $n_1^{rr} = n_2^{rr}$ and $H_2 = +\mathcal{M}H_1^*\mathcal{M}$. Together with the spectral-reflection symmetry, this implies that the rainbow state $(\mathcal{P}_1 \otimes \mathcal{P}_2)|Z\rangle$ is an eigenstate of $H_1 + H_2$.

This state is also an eigenstate of the coupling, and therefore of the overall H in Eq. (6). Such a rainbow state exists for each subsector satisfying $\mathcal{P}_1 = \mathcal{M}\mathcal{P}_2\mathcal{M}$, leading to an equally spaced tower of scar states with energies $V_0/4\tilde{a}^6 + 2V_0 n_1^{rr}$. We emphasize this tower is *distinct* from the strictly sub-volume-law scars of the PXP model, which reside in the sector with $n_1^{rr} = n_2^{rr} = 0$ [23,25]. This tower of states becomes exact in the limit $V_{i,i+1} \gg \Omega \gg V_{i,i+2}$; remarkably, it is also robust away from this limit.

In Fig. 4(b), we determine the maximum overlap between each eigenstate and the projection of $|Z\rangle$ into the $n_1^{rr} = n_2^{rr} = 0$ sector. For strictly nearest-neighbor interactions (blue), the maximum overlap asymptotes to unity as $V_0 \rightarrow \infty$. However, this is not the case when the full van der Waals interaction is accounted for (red); here, the overlap grows slowly, never exceeding ~ 0.5 . This is a result of the next-nearest-neighbor interactions breaking the spectral-reflection symmetry of $H_{1,2}$ in Eq. (6).

Figure 4(c) shows the quench dynamics of the $|Z\rangle$ rainbow state under the Hamiltonian Eq. (5). We consider both nearest-neighbor (blue) and full van der Waals interactions (red) with parameters $V_0 = 12\Omega$ and interchain spacing $\tilde{a} \sim 1.51$. Remarkably, for nearest-neighbor interactions, the oscillations are robust, persisting well beyond the local thermalization timescale $1/\Omega$. In the limit $V_0 \rightarrow \infty$, the coherent dynamics become exactly periodic with a period $\tau = \pi/V_0$ as a consequence of the rainbow tower. Including long-range interactions leads to faster relaxation dominated by next-nearest-neighbor terms on a timescale $1/V_{i,i+2}$. This dynamical behavior is confirmed by measuring the average expectation value between inversion partners $\langle \sigma_i^x(t) \sigma_i^x(t) \rangle = \sum_i \langle \sigma_i^x(t) \sigma_i^x(t) \rangle / 2N$. Interestingly, the sub-volume-law scars of the PXP model [23,24] coexist with the rainbow scars, still displaying a strong dynamical signature, illustrated in Fig. 4(d) by preparing the system in the Néel state. We emphasize that the dynamical signature of the rainbow tower is more robust than that of the PXP scars for nearest-neighbor interactions. This results from the fact that $|Z\rangle$ has unit overlap with the rainbow tower in the limit $V_0 \rightarrow \infty$, whereas the PXP tower remains approximate in this limit. In Ref. [72] we explored various perturbations to Eq. (5), as well as a translation-invariant model in which a similar dynamical signature was found.

Experimental preparation. Rainbow-state preparation requires nonlocal gates to entangle inversion partners at sites i and \tilde{i} , posing an experimental challenge. Recently, however, the rainbow state was prepared in a trapped ion quantum simulator [88]. We recognize that these systems are able to apply nonlocal two-body entangling gates, allowing for easier preparation, but experimental groups are attempting to implement similar gates in Rydberg arrays. A possible solution is quantum state reversal [89–91]. Alternatively, in a ladder geometry, the Rydberg system becomes translation-invariant, and state preparation is local. In Ref. [72] we found the nonergodic dynamics to persist in this geometry.

Conclusion. This work gives a general recipe to realize a new class of QMBS, dubbed rainbow scars, that are related to the infinite-temperature thermofield double states. Rainbow scars emerge in any system of the form (1), provided (i) $H_2 =$

$-\mathcal{M}H_1^*\mathcal{M}$ and (ii) Eq. (2) is an eigenstate of the coupling V_c . Symmetries enrich the construction, leading to multiple or even towers of rainbow scars with a rich group structure. These nonthermal states display volume-law entanglement for random bipartitions and sub-volume-law scaling for a fine-tuned bipartition, as well as perfect coherent dynamics in the presence of towers. Our work serves as an experimental blueprint for Rydberg simulators, where we find a robust dynamical signature distinct from previous studies.

Acknowledgments. We thank Adam Kaufman for insightful discussions on the experimental possibilities in the Rydberg system. Z.-C.Y. and A.V.G. acknowledge funding by AFOSR, AFOSR MURI, DoE ASCR Quantum Testbed

Pathfinder program (Award No. DE-SC0019040), DoE QSA, NSF QLCI (Award No. OMA-2120757), U.S. Department of Energy Award No. DE-SC0019449, DoE ASCR Accelerated Research in Quantum Computing program (Award No. DE-SC0020312), ARO MURI, and DARPA SAVaNT ADVENT. T.I. and S.X. acknowledge the hospitality of the Aspen Center for Physics, which is supported by National Science Foundation Grant No. PHY-1607611. S.X. also thanks the hospitality of KITP supported by the National Science Foundation under Grant No. NSF PHY-1748958. Portions of this research were conducted with the advanced computing resources provided by Texas A&M High Performance Research Computing.

-
- [1] J. M. Deutsch, *Phys. Rev. A* **43**, 2046 (1991).
 [2] M. Srednicki, *Phys. Rev. E* **50**, 888 (1994).
 [3] M. Rigol and M. Srednicki, *Phys. Rev. Lett.* **108**, 110601 (2012).
 [4] A. Polkovnikov, K. Sengupta, A. Silva, and M. Vengalattore, *Rev. Mod. Phys.* **83**, 863 (2011).
 [5] T. Kinoshita, T. Wenger, and D. S. Weiss, *Nature (London)* **440**, 900 (2006).
 [6] P. Calabrese, F. H. L. Essler, and M. Fagotti, *Phys. Rev. Lett.* **106**, 227203 (2011).
 [7] R. Nandkishore and D. A. Huse, *Annu. Rev. Condens. Matter Phys.* **6**, 15 (2015).
 [8] D. A. Abanin, E. Altman, I. Bloch, and M. Serbyn, *Rev. Mod. Phys.* **91**, 021001 (2019).
 [9] A. Pal and D. A. Huse, *Phys. Rev. B* **82**, 174411 (2010).
 [10] J.-Y. Choi, S. Hild, J. Zeiher, P. Schauß, A. Rubio-Abadal, T. Yefsah, V. Khemani, D. A. Huse, I. Bloch, and C. Gross, *Science* **352**, 1547 (2016).
 [11] A. M. Kaufman, M. E. Tai, A. Lukin, M. Rispoli, R. Schittko, P. M. Preiss, and M. Greiner, *Science* **353**, 794 (2016).
 [12] M. Rispoli, A. Lukin, R. Schittko, S. Kim, M. E. Tai, J. Léonard, and M. Greiner, *Nature (London)* **573**, 385 (2019).
 [13] P. N. Jepsen, W. W. Ho, J. Amato-Grill, I. Dimitrova, E. Demler, and W. Ketterle, *Phys. Rev. X* **11**, 041054 (2021).
 [14] A. Mazurenko, C. S. Chiu, G. Ji, M. F. Parsons, M. Kanász-Nagy, R. Schmidt, F. Grusdt, E. Demler, D. Greif, and M. Greiner, *Nature (London)* **545**, 462 (2017).
 [15] H. Levine, A. Keesling, A. Omran, H. Bernien, S. Schwartz, A. S. Zibrov, M. Endres, M. Greiner, V. Vuletić, and M. D. Lukin, *Phys. Rev. Lett.* **121**, 123603 (2018).
 [16] P. Scholl, M. Schuler, H. J. Williams, A. A. Eberharter, D. Barredo, K.-N. Schymik, V. Lienhard, L.-P. Henry, T. C. Lang, T. Lahaye, A. M. Läuchli, and A. Browaeys, *Nature (London)* **595**, 233 (2021).
 [17] M. K. Joshi, A. Elben, B. Vermersch, T. Brydges, C. Maier, P. Zoller, R. Blatt, and C. F. Roos, *Phys. Rev. Lett.* **124**, 240505 (2020).
 [18] C. Monroe, W. C. Campbell, L.-M. Duan, Z.-X. Gong, A. V. Gorshkov, P. W. Hess, R. Islam, K. Kim, N. M. Linke, G. Pagano, P. Richerme, C. Senko, and N. Y. Yao, *Rev. Mod. Phys.* **93**, 025001 (2021).
 [19] X. Mi, P. Roushan, C. Quintana, S. Mandra, J. Marshall, C. Neill, F. Arute, K. Arya, J. Atalaya, R. Babbush *et al.*, *Science* **374**, 1479 (2021).
 [20] J. I. Colless, V. V. Ramasesh, D. Dahlen, M. S. Blok, M. E. Kimchi-Schwartz, J. R. McClean, J. Carter, W. A. de Jong, and I. Siddiqi, *Phys. Rev. X* **8**, 011021 (2018).
 [21] H. Bernien, S. Schwartz, A. Keesling, H. Levine, A. Omran, H. Pichler, S. Choi, A. S. Zibrov, M. Endres, M. Greiner *et al.*, *Nature (London)* **551**, 579 (2017).
 [22] D. Bluvstein, A. Omran, H. Levine, A. Keesling, G. Semeghini, S. Ebadi, T. Wang, A. Michailidis, N. Maskara, W. Ho, S. Choi, M. Serbyn, M. Greiner, V. Vuleti, and M. D. Lukin, *Science* **371**, 1355 (2021).
 [23] C. J. Turner, A. A. Michailidis, D. A. Abanin, M. Serbyn, and Z. Papić, *Nat. Phys.* **14**, 745 (2018).
 [24] C. J. Turner, A. A. Michailidis, D. A. Abanin, M. Serbyn, and Z. Papić, *Phys. Rev. B* **98**, 155134 (2018).
 [25] M. Serbyn, D. A. Abanin, and Z. Papić, *Nat. Phys.* **17**, 675 (2021).
 [26] S. Moudgalya, S. Rachel, B. A. Bernevig, and N. Regnault, *Phys. Rev. B* **98**, 235155 (2018).
 [27] S. Moudgalya, N. Regnault, and B. A. Bernevig, *Phys. Rev. B* **98**, 235156 (2018).
 [28] S. Choi, C. J. Turner, H. Pichler, W. W. Ho, A. A. Michailidis, Z. Papić, M. Serbyn, M. D. Lukin, and D. A. Abanin, *Phys. Rev. Lett.* **122**, 220603 (2019).
 [29] W. W. Ho, S. Choi, H. Pichler, and M. D. Lukin, *Phys. Rev. Lett.* **122**, 040603 (2019).
 [30] V. Khemani, C. R. Laumann, and A. Chandran, *Phys. Rev. B* **99**, 161101(R) (2019).
 [31] C.-J. Lin and O. I. Motrunich, *Phys. Rev. Lett.* **122**, 173401 (2019).
 [32] T. Iadecola, M. Schechter, and S. Xu, *Phys. Rev. B* **100**, 184312 (2019).
 [33] M. Schechter and T. Iadecola, *Phys. Rev. Lett.* **123**, 147201 (2019).
 [34] S. Chattopadhyay, H. Pichler, M. D. Lukin, and W. W. Ho, *Phys. Rev. B* **101**, 174308 (2020).
 [35] S. Moudgalya, N. Regnault, and B. A. Bernevig, *Phys. Rev. B* **102**, 085140 (2020).
 [36] D. K. Mark and O. I. Motrunich, *Phys. Rev. B* **102**, 075132 (2020).
 [37] S. Pai and M. Pretko, *Phys. Rev. Lett.* **123**, 136401 (2019).
 [38] S. Sugiura, T. Kuwahara, and K. Saito, *Phys. Rev. Research* **3**, L012010 (2021).
 [39] A. Haldar, D. Sen, R. Moessner, and A. Das, *Phys. Rev. X* **11**, 021008 (2021).

- [40] B. Mukherjee, S. Nandy, A. Sen, D. Sen, and K. Sengupta, *Phys. Rev. B* **101**, 245107 (2020).
- [41] T. Iadecola and S. Vijay, *Phys. Rev. B* **102**, 180302(R) (2020).
- [42] S. Moudgalya, B. A. Bernevig, and N. Regnault, *Phys. Rev. B* **102**, 195150 (2020).
- [43] K. Bull, I. Martin, and Z. Papić, *Phys. Rev. Lett.* **123**, 030601 (2019).
- [44] T. Iadecola and M. Schechter, *Phys. Rev. B* **101**, 024306 (2020).
- [45] A. A. Michailidis, C. J. Turner, Z. Papić, D. A. Abanin, and M. Serbyn, *Phys. Rev. X* **10**, 011055 (2020).
- [46] J. Wildeboer, A. Seidel, N. S. Srivatsa, A. E. B. Nielsen, and O. Erten, *Phys. Rev. B* **104**, L121103 (2021).
- [47] N. S. Srivatsa, J. Wildeboer, A. Seidel, and A. E. B. Nielsen, *Phys. Rev. B* **102**, 235106 (2020).
- [48] Y. Kuno, T. Mizoguchi, and Y. Hatsugai, *Phys. Rev. B* **102**, 241115(R) (2020).
- [49] P. A. McClarty, M. Haque, A. Sen, and J. Richter, *Phys. Rev. B* **102**, 224303 (2020).
- [50] D. Banerjee and A. Sen, *Phys. Rev. Lett.* **126**, 220601 (2021).
- [51] C. M. Langlett and S. Xu, *Phys. Rev. B* **103**, L220304 (2021).
- [52] H. Zhao, A. Smith, F. Mintert, and J. Knolle, *Phys. Rev. Lett.* **127**, 150601 (2021).
- [53] J. Ren, C. Liang, and C. Fang, *Phys. Rev. Lett.* **126**, 120604 (2021).
- [54] D. K. Mark, C.-J. Lin, and O. I. Motrunich, *Phys. Rev. B* **101**, 195131 (2020).
- [55] N. O’Dea, F. Burnell, A. Chandran, and V. Khemani, *Phys. Rev. Research* **2**, 043305 (2020).
- [56] K. Pakrouski, P. N. Pallegar, F. K. Popov, and I. R. Klebanov, *Phys. Rev. Lett.* **125**, 230602 (2020).
- [57] K. Pakrouski, P. N. Pallegar, F. K. Popov, and I. R. Klebanov, *Phys. Rev. Research* **3**, 043156 (2021).
- [58] S. Moudgalya, E. O’Brien, B. A. Bernevig, P. Fendley, and N. Regnault, *Phys. Rev. B* **102**, 085120 (2020).
- [59] N. Shiraishi, *J. Stat. Mech.: Theory Exp.* (2019) 083103.
- [60] N. Shiraishi and T. Mori, *Phys. Rev. Lett.* **119**, 030601 (2017).
- [61] G. Ramírez, J. Rodríguez-Laguna, and G. Sierra, *J. Stat. Mech.: Theory Exp.* (2015) P06002.
- [62] G. Ramírez, J. Rodríguez-Laguna, and G. Sierra, *J. Stat. Mech.: Theory Exp.* (2014) P10004.
- [63] G. Vitagliano, A. Riera, and J. I. Latorre, *New J. Phys.* **12**, 113049 (2010).
- [64] The construction Eq. (1) is valid for arbitrary dimensions, where the mirror-symmetry operator \mathcal{M} is the map $\mathcal{M} : i \rightarrow \bar{i}$. For concreteness we restrict ourselves to one-dimensional systems.
- [65] W. Cottrell, B. Freivogel, D. M. Hofman, and S. F. Lokhande, *J. High Energy Phys.* **02** (2019) 058.
- [66] T. Hartman and J. Maldacena, *J. High Energy Phys.* **05** (2013) 014.
- [67] K. Papadodimas and S. Raju, *Phys. Rev. Lett.* **115**, 211601 (2015).
- [68] J. Maldacena, *J. High Energy Phys.* **04** (2003) 021.
- [69] T. Schuster, B. Kobrin, P. Gao, I. Cong, E. T. Khabiboulline, N. M. Linke, M. D. Lukin, C. Monroe, B. Yoshida, and N. Y. Yao, [arXiv:2102.00010](https://arxiv.org/abs/2102.00010).
- [70] S. Nezami, H. W. Lin, A. R. Brown, H. Gharibyan, S. Leichenauer, G. Salton, L. Susskind, B. Swingle, and M. Walter, [arXiv:2102.01064](https://arxiv.org/abs/2102.01064).
- [71] A. R. Brown, H. Gharibyan, S. Leichenauer, H. W. Lin, S. Nezami, G. Salton, L. Susskind, B. Swingle, and M. Walter, [arXiv:1911.06314](https://arxiv.org/abs/1911.06314).
- [72] See Supplemental Material at <http://link.aps.org/supplemental/10.1103/PhysRevB.105.L060301> for a discussion on the entanglement scaling of the rainbow-state and results on nonergodic dynamics due to rainbow scars for a rydberg system in the ladder geometry.
- [73] M.-D. Choi, *Linear Algebra Appl.* **10**, 285 (1975).
- [74] A. Jamiolkowski, *Rep. Math. Phys.* **3**, 275 (1972).
- [75] D. N. Page, *Phys. Rev. Lett.* **71**, 1291 (1993).
- [76] H. Liu and S. Vardhan, *J. High Energy Phys.* **03** (2021) 088.
- [77] D. Faiez and D. Šafránek, *Phys. Rev. B* **101**, 060401(R) (2020).
- [78] H. Fujita, Y. O. Nakagawa, S. Sugiura, and M. Watanabe, *J. High Energy Phys.* **12** (2018) 112.
- [79] E. Bianchi and P. Donà, *Phys. Rev. D* **100**, 105010 (2019).
- [80] V. Oganesyan and D. A. Huse, *Phys. Rev. B* **75**, 155111 (2007).
- [81] P. Sierant and J. Zakrzewski, *Phys. Rev. B* **101**, 104201 (2020).
- [82] W. Buijsman, V. Cheianov, and V. Gritsev, *Phys. Rev. Lett.* **122**, 180601 (2019).
- [83] Y. Y. Atas, E. Bogomolny, O. Giraud, and G. Roux, *Phys. Rev. Lett.* **110**, 084101 (2013).
- [84] M. Schechter and T. Iadecola, *Phys. Rev. B* **98**, 035139 (2018).
- [85] We note that if $J_x = J_y = J_z$ the Hamiltonian acquires an SU(2) symmetry leading to a larger rainbow scar tower. In this circumstance each state is connected with different raising operators satisfying different commutation relations.
- [86] C.-J. Lin, A. Chandran, and O. I. Motrunich, *Phys. Rev. Research* **2**, 033044 (2020).
- [87] Here the projection operators, $\mathcal{P}_{1(2)}$ commute with the spectral-symmetry generators, i.e., $[\mathcal{P}_{1(2)}, \mathcal{O}^\pm] = 0$.
- [88] D. Zhu, S. Johri, N. Linke, K. Landsman, C. H. Alderete, N. Nguyen, A. Matsuura, T. Hsieh, and C. Monroe, *Proc. Natl. Acad. Sci.* **117**, 25402 (2020).
- [89] S. Bose, *Phys. Rev. Lett.* **91**, 207901 (2003).
- [90] C. Albanese, M. Christandl, N. Datta, and A. Ekert, *Phys. Rev. Lett.* **93**, 230502 (2004).
- [91] A. Bapat, E. Schoute, A. V. Gorshkov, and A. M. Childs, [arXiv:2003.02843](https://arxiv.org/abs/2003.02843).